Alluvial Stratigraphic Response to Abruptly Increasing and Variable Sediment Supply Insights From Stratigraphic Forward Modeling

Wang, Youwei; Abels, Hemmo A.

DOI
10.1029/2025GL115985

Publication date
2025

Document Version
Final published version

Published in
Geophysical Research Letters

AGU ADVANCING EARTH AND SPACE SCIENCES

Geophysical Research Letters

RESEARCH LETTER
10.1029/2025GL115985

Alluvial Stratigraphic Response to Abruptly Increasing and Variable Sediment Supply: Insights From Stratigraphic Forward Modeling

Youwei Wang[1,2] **and Hemmo A. Abels**[3]

[1]State Key Laboratory of Lithospheric and Environmental Coevolution, Institute of Geology and Geophysics, Chinese Academy of Sciences, Beijing, China, [2]Department of Geography, University of California Santa Barbara, Santa Barbara, CA, USA, [3]Department of Geosciences and Engineering, Delft University of Technology, Delft, Netherlands

Abstract Understanding how alluvial stratigraphy responds to sediment supply perturbations is critical for interpreting past environmental changes from the sedimentary record, characterizing subsurface reservoirs, and forecasting future landscape evolution. However, identifying and quantifying sediment supply signals preserved in the rock record remain challenging, leaving their stratigraphic imprint insufficiently understood. To help address this issue, we use a process-based numerical model to simulate alluvial stratigraphy under different sediment supply scenarios, independently testing the effects of supply magnitude and variability. Our results show that sediment supply variability has a stronger impact than magnitude: increased variability leads to much thicker channel-belt deposits and elevated yet alternating high and low down-valley slopes. In contrast, greater total sediment supply results in only slightly thicker channel-belt deposits and uniformly elevated down-valley slopes. These results reconcile diverse fluvial stratigraphic responses to sediment-supply changes across basins during climatic perturbations.

Plain Language Summary This study uses a computer model to explore how sediment supply changes affect rock records. We tested two key changes: (a) the total amount of sediment increases by 40% and (b) the sediment flux becomes more variable without total supply changes. Our findings show that variable sediment flux leads to thicker channel-belt deposits and alternating higher and lower down-valley slopes, while increased total sediment supply causes uniformly steeper down-valley slopes without changing channel size much. These results help improve our understanding of past environmental changes and can guide predictions of how river landscapes are preserved in the subsurface.

Key Points:

- Enhanced sediment supply variability leads to larger channel belt thickness and alternating high and low down-valley slopes
- Increased total sediment supply generates uniformly elevated down-valley slopes with limited impact on channel belt thickness
- Stratigraphic signatures of different sediment input profiles help constrain paleoenvironmental interpretations and reservoir predictions

Supporting Information:

Supporting Information may be found in the online version of this article.

Correspondence to:

Y. Wang,
youweiwang@mail.iggcas.ac.cn

Citation:

Wang, Y., & Abels, H. A. (2025). Alluvial stratigraphic response to abruptly increasing and variable sediment supply: Insights from stratigraphic forward modeling. *Geophysical Research Letters*, *52*, e2025GL115985. https://doi.org/10.1029/2025GL115985

Received 10 APR 2025
Accepted 26 AUG 2025

Author Contributions:

Conceptualization: Youwei Wang, Hemmo A. Abels
Data curation: Youwei Wang
Formal analysis: Youwei Wang
Funding acquisition: Hemmo A. Abels
Investigation: Youwei Wang, Hemmo A. Abels
Methodology: Youwei Wang, Hemmo A. Abels
Project administration: Hemmo A. Abels
Resources: Hemmo A. Abels
Software: Youwei Wang
Supervision: Hemmo A. Abels
Validation: Youwei Wang, Hemmo A. Abels
Visualization: Youwei Wang

1. Introduction

Alluvial stratigraphy results from complex interactions between external forcings (e.g., climate and tectonics) and autogenic processes (e.g., channel avulsion and lateral migration) (Hajek & Straub, 2017). Sequence stratigraphy has long acknowledged both accommodation and sediment supply as co-equal controls (Bridge & Leeder, 1979; Burgess et al., 2019; Catuneanu et al., 2011; Muto & Steel, 1997; Neal & Abreu, 2009; Shanley & McCabe, 1994; Straub & Wang, 2013), yet quantitative assessments of upstream sediment supply (Q_s) variations in fully fluvial settings remain relatively scarce (Armitage et al., 2013; Blum & Törnqvist, 2000; Sharma et al., 2024; Simpson & Castelltort, 2012; Wang et al., 2021, 2023, 2024). Over geological timescales, Q_s varies with climatic fluctuations driving precipitation and weathering/erosion changes, and with tectonic activity rejuvenating source areas (Allen et al., 2013; Armitage et al., 2011, 2013; Castelltort & Van Den Driessche, 2003; Duller et al., 2019; Romans et al., 2016; Syvitski et al., 2000). Yet, these signals are often obscured by "signal shredding" wherein autogenic processes can mask sediment supply changes (Jerolmack & Paola, 2010). Only substantial or persistent perturbations could leave their signatures in stratigraphy (Duller et al., 2019; Foreman & Straub, 2017; Romans et al., 2016; Straub et al., 2020; Toby et al., 2019).

The Paleocene–Eocene Thermal Maximum (PETM, ~56 Ma) (Zachos et al., 2010) exemplifies these complexities. During the PETM, channel sand-body widths increased markedly in the Bighorn and Tremp Basins—up to tenfold and eightfold, respectively—while channel depths varied, with a fourfold increase in the Bighorn Basin and minimal change in the Piceance and Hanna Basins (Barefoot et al., 2022; Chen et al., 2018; Dechesne et al., 2020; Foreman, 2014; Foreman et al., 2012). Minimal changes in aggradation rates in the axial Bighorn Basin indicate that tectonic forcing was not the primary driver (van der Meulen et al., 2020). Additional evidence

Writing – original draft: Youwei Wang
Writing – review & editing: Youwei Wang, Hemmo A. Abels

for varying sediment supply regimes includes enhanced channel mobility through increased bar and floodplain reworking (Barefoot et al., 2022; Prieur et al., 2024, 2025), downstream expansion of coarser facies with elevated down-valley slopes (Pujalte et al., 2015), and preferential clay mineral enrichment on the continental margin (Podrecca et al., 2021).

Two contrasting hypotheses have been proposed to explain these PETM fluvial responses: (a) a sustained increase in sediment flux from enhanced chemical weathering and erosion (Carmichael et al., 2017; Chen et al., 2018; Foreman et al., 2012; Jin et al., 2022; Schmitz & Pujalte, 2007; Sharman et al., 2022; Tierney et al., 2022; Vimpere et al., 2023); (b) increased sediment variability, where extreme flow events mobilize sediment in pulses without altering the long-term flux (Barefoot et al., 2022; Prieur et al., 2024). To distinguish these two contrasting scenarios, we use stratigraphic forward modeling to analyze the impacts of stepwise sediment flux increase and amplified sediment flux variability on stratigraphic architecture, channel belt thickness, and down-valley slope adjustments. With these, we can identify diagnostic criteria that link sediment-supply changes to observable stratigraphic patterns.

2. Methodology

2.1. Process-Based Numerical Alluvial Stratigraphic Model

We employed the Karssenberg and Bridge (2008) model to simulate basin-scale landscape evolution and alluvial stratigraphy. The model accounts for sediment transport, erosion, and deposition within a network of channel belts and floodplains, with sediment and water transport following a diffusion equation, wherein the transport rate depends on local water discharge.

Channel-belt bifurcation is represented by two processes: purely stochastic events and a dependent mechanism driven by the relative advantage of cross-valley slope (S_{cv}) over down-valley slope (S_{dv}) and by flood discharge (Q_w) exceedance of a threshold discharge value (Q_a). At each grid cell and time step, the probability of a dependent bifurcation is

$$\mathrm{P\,(B)} = \left(\frac{Q_w}{Q_a}\right)^{e_Q}\left(k_s\frac{S_{cv}}{S_{dv}}\right)^{e_s} \quad (1)$$

where k_s is the slope proportionality constant, e_Q is the threshold discharge component, and e_s is the slope exponent (Karssenberg & Bridge, 2008; Mackey & Bridge, 1995).

A bifurcation occurs if P(B) exceeds a draw from the uniform distribution U (0, 1). Upon bifurcation, the upstream discharge q_0 is apportioned into branch discharges q_1 and q_2 in proportion to their gradients s_1 and s_2, each perturbed by Gaussian noise $n_i \sim$ N (0, σ^2). If either branch fraction q_i/q_0 falls below the critical threshold $u_{crit} = 0.4$, a bifurcation turns into an avulsion (Karssenberg & Bridge, 2008). Values of other unspecified parameters are listed in Supporting Information S1 Table S1.

Channel belt aggradation and degradation are computed via the sediment continuity equation. Channel belt width increases with Q_s over time until the avulsion threshold is reached, which is a simplification, since channel belt widening in natural systems reduces boundary shear stress toward the critical value for sediment motion (Limaye, 2020). Floodplain aggradation initiates when local elevations fall below adjacent channel belts and is modeled by sediment diffusion–advection. Model sensitivity to varied water discharge (Q_w) and sediment supply (Q_s) is detailed in Wang et al. (2021).

2.2. Model Set-Up and Scenarios

The modeled basin is a 60-km (down-valley) by 40-km (cross-valley) rectangular domain discretized into 200 m × 200 m cells (Figure 1). The initial topography features a gentle down-valley slope (S_0) of 1.1×10^{-4}, calibrated to achieve a graded alluvial profile under steady-state conditions with a constant water discharge (Q_{w0}) of 7.9×10^{10} m^3/year and a constant sediment supply (Q_{s0}) of 1.0×10^6 m^3/year (Wang et al., 2021). A steady sea-level rise of 0.4 m/kyr simulates long-term accommodation, which aligns with field-measured aggradation rates (Abels et al., 2012).

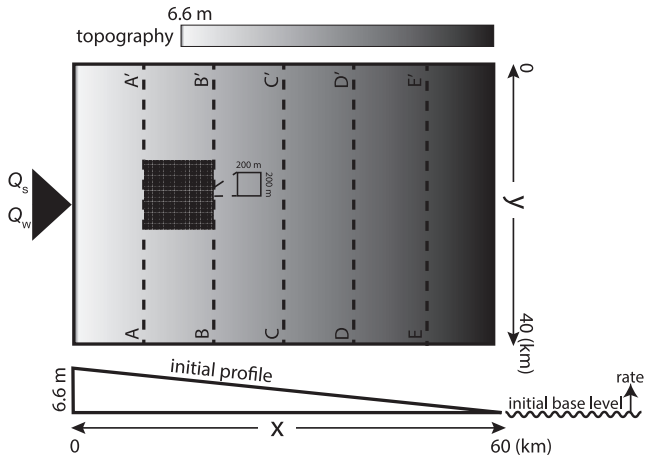

Figure 1. Initial alluvial plain shown in plan view (top) and as a longitudinal profile along the basin axis (bottom). The domain, discretized into 200 m × 200 m cells, spans 40 km cross-basin and 60 km along the basin. Cross-sectional profiles are extracted along line BB', and downstream sections are taken along the basin axis at $y = 20$ km. Modified from Wang et al. (2021).

Over geological timescales, Q_s responds exponentially to changes in Q_w (Syvitski et al., 2000). Significant variations in Q_w can lead to extreme variability in Q_s, with recent syn-PETM estimates 2–4 times greater than pre- and post-PETM counterparts (Prieur et al., 2025; Sømme et al., 2023). However, the KB08 model cannot accommodate such extreme Q_s variability. Furthermore, Wang et al. (2021) demonstrated that the model is more sensitive to the Q_s/Q_w ratio, rather than to the absolute values of either Q_w or Q_s alone, consistent with previous findings (Bryant et al., 1995; Zhang et al., 2019).

To isolate sediment supply effects and ensure computational stability, we keep Q_w constant while varying Q_s. Each 40-kyr simulation (1-year time steps) spans three phases: pre-event (0–10 kyr), event (10–30 kyr), and post-event (30–40 kyr). The baseline scenario reflects undisturbed conditions (Figure 2a); the second scenario imposes an abrupt 40% increase in Q_s during the event phase, a value consistent with the 20%–50% variability in Q_s predicted under Milankovitch-scale climate forcing (Blum & Hattier-Womack, 2009Blum & Hattier-Womack, 2009) (Figure 3a); in the third scenario, Q_s alternates ±40% around its baseline in 5 kyr square-wave cycles during the event −2.5 kyr at 1.4 Q_s, then 2.5 kyr at 0.6 Q_s, yielding unchanged total Q_s (Figure 3e); and a fourth intermediate scenario combines increased supply with moderate variability (Q_s alternates between 1.2 Q_s and 1.4 Q_s; Figure 4a). All other parameters follow Wang et al. (2021) (Table S1 in Supporting Information S1).

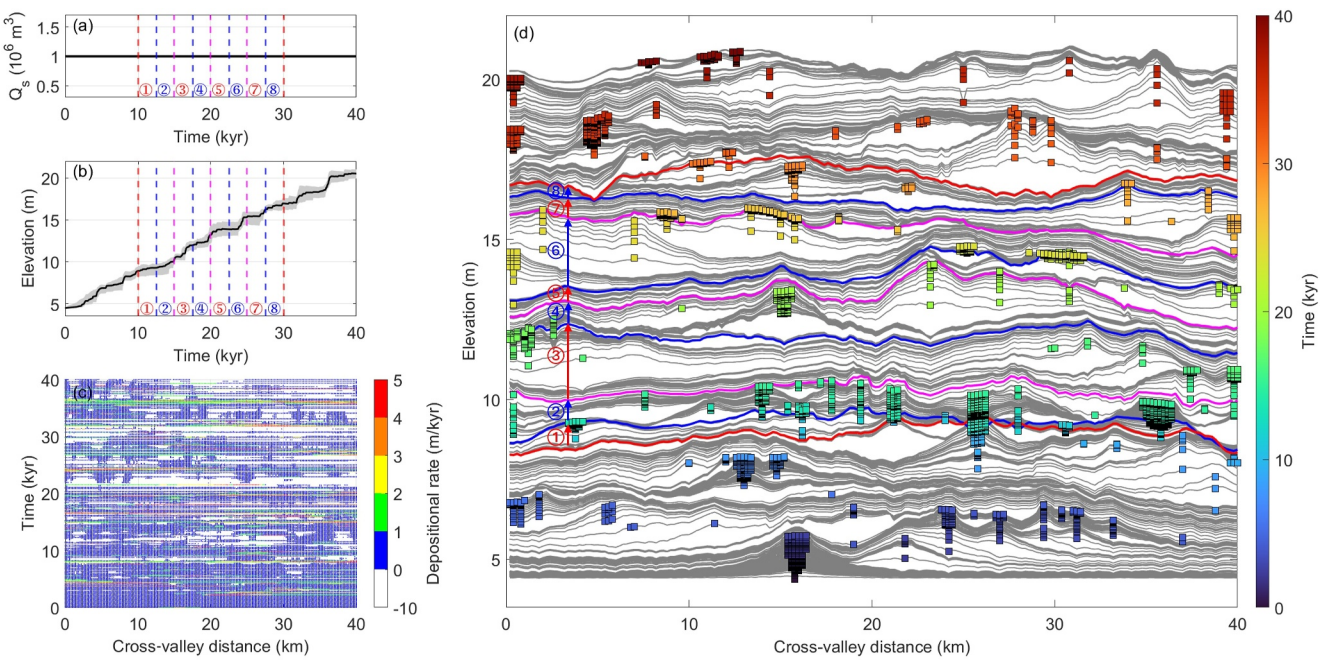

Figure 2. Alluvial stratigraphy at cross section along line BB' (Figure 1) of the baseline scenario. (a) Temporal evolution of sediment supply (Q_s). (b) Variation in surface topography: gray lines indicate the topographic range, and the solid line shows the average elevation. (c) Chronostratigraphic diagram showing spatial and temporal variability in depositional rates, with white areas denoting degradation and colored dots marking episodes of aggradation. (d) Cross-section surface topography, with a time interval of 50 years. Closely spaced timelines indicate periods of low to no deposition, while crosscutting signifies erosion. Colored squares mark channel positions (not dimensions). Red lines delimit the event phase (10–30 kyr). Blue and magenta lines correspond to topography at the time shown in panels (a) and (b). Upward and downward arrows beside circled numbers indicate aggradation and degradation, respectively.

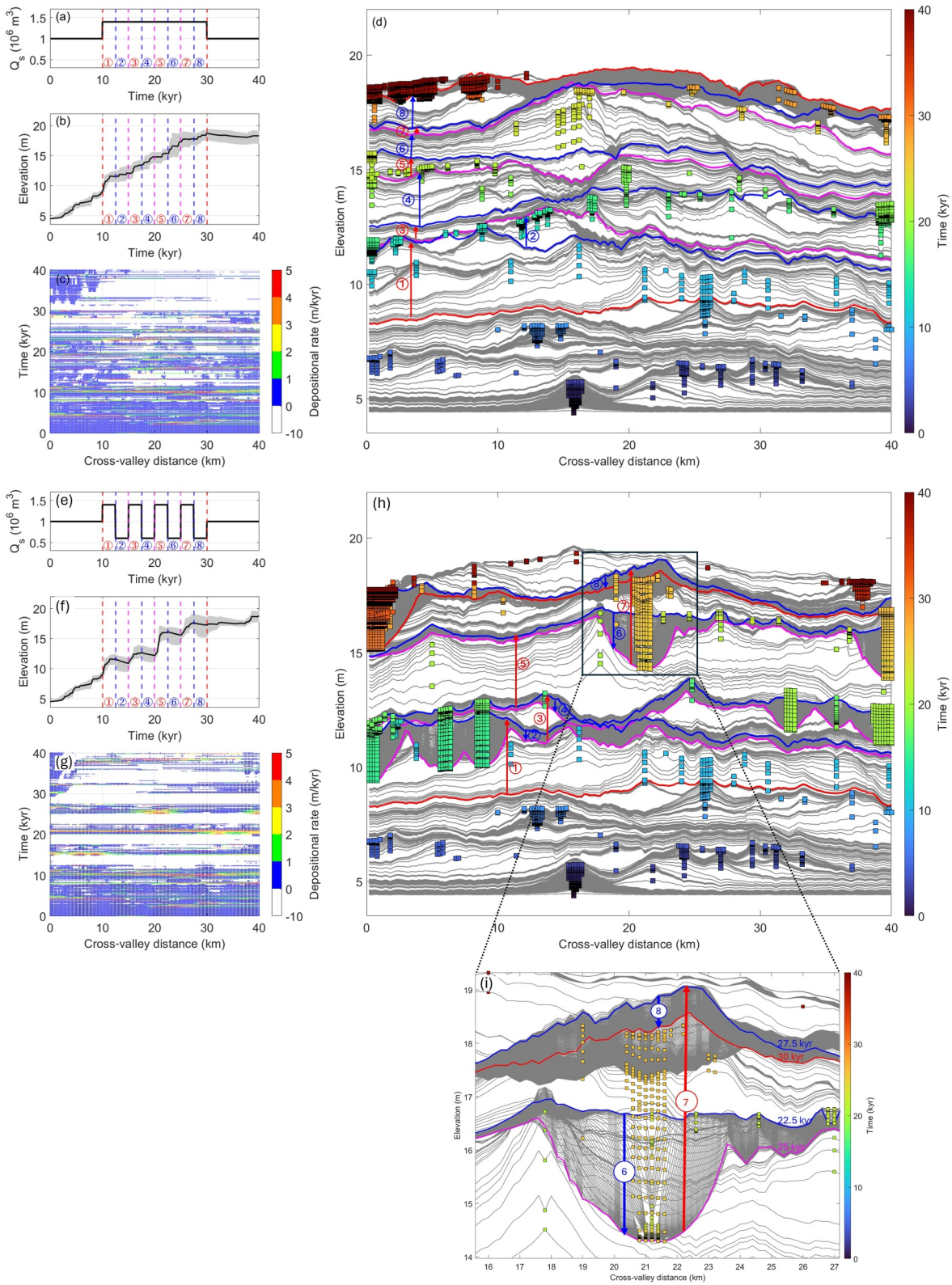

Figure 3. Alluvial stratigraphic patterns at cross sections along line BB' of (a–d) the increased sediment supply scenario and (e–i) the variable sediment supply scenario. For subplot element details, see Figure 2. Panel (i) offers an enlarged view of the region highlighted by the black rectangle in Panel (g). In Panels (h) and (i), downward-pointing blue arrows, in conjunction with magenta lines below blue lines (i.e., later times plot below earlier times), demonstrate regional erosion during the corresponding periods.

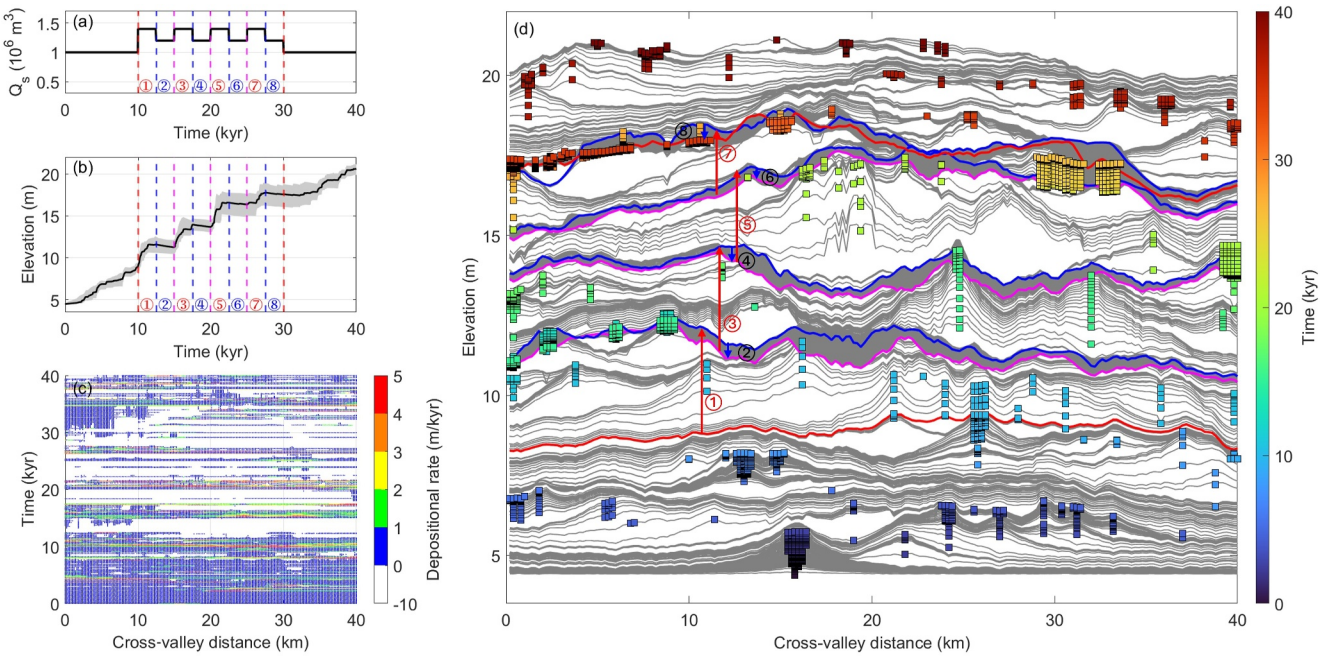

Figure 4. Alluvial stratigraphic patterns at cross section along line BB' of the intermediate scenario with increased total sediment supply and slight temporal variability. For subplot element details, see Figure 2.

2.3. Model Output Analyses

We evaluate stratigraphic architecture by analyzing surface elevation timelines (e.g., Figure 2d)—where cross-cutting indicates erosion, condensed timelines suggest minimal deposition, and wide spacing means rapid aggradation—and by constructing chronostratigraphic diagrams (e.g., Figure 2c).

Channel belt thickness is derived from detrended relative topography using the progressive black top hat (PBTH) algorithm (Luo et al., 2015). For each 2–6 km sliding window, a pre-incision surface is first reconstructed and subtracted from the elevation profile to yield incision depths, retaining only values above robust thresholds (Text S1, Figure S1 in Supporting Information S1, Movies S1–S4). These PBTH values serve as a relative index of depositional magnitude and are not directly equivalent to absolute field measurements. Additionally, we evaluate distributional differences between channel-belt thickness distributions using two-sample Kolmogorov-Smirnov tests (Conover, 1999), with $p \ll 0.01$ denoting statistical significance.

Down-valley slopes are calculated as elevation differences over 10-km segments along the basin axis ($y = 20$ km in Figure 1), normalized by the initial down-valley slope S_0 to yield a dimensionless metric (S^*), which is visualized as a heat map (e.g., Figure 5d). We further assess the spatial evolution of S^* by averaging profiles over 2.5-kyr intervals (e.g., Figure 5e) and tracking the temporal evolution of spatially averaged S^* from 10 to 50 km down-valley (e.g., Figure 5f).

3. Results

3.1. Alluvial Stratigraphic Architecture

Across all scenarios, stratigraphic patterns reflect sensitivity to interactions between sediment supply, accommodation creation, and autogenic processes. Hereafter, we analyze patterns using cross sections along a line from the upstream side, the line BB' (Figure 1) as an example. In the baseline scenario, the basin experiences relatively uniform aggradation indicated by gradual elevation increase, spatially and temporally stochastic deposition, and episodic autogenic erosion, presenting overall compensational stacking behaviors and stochastic distributions of channel belts (Figures 2b–2d). The increased sediment supply scenario yields enhanced aggradation, particularly noticeable at the event onset at 10 kyr, causing steeper topographic gradients and initially rapid deposition (Figures 3b–3d). The subsequent reduction in available accommodation results in increased erosion in the later

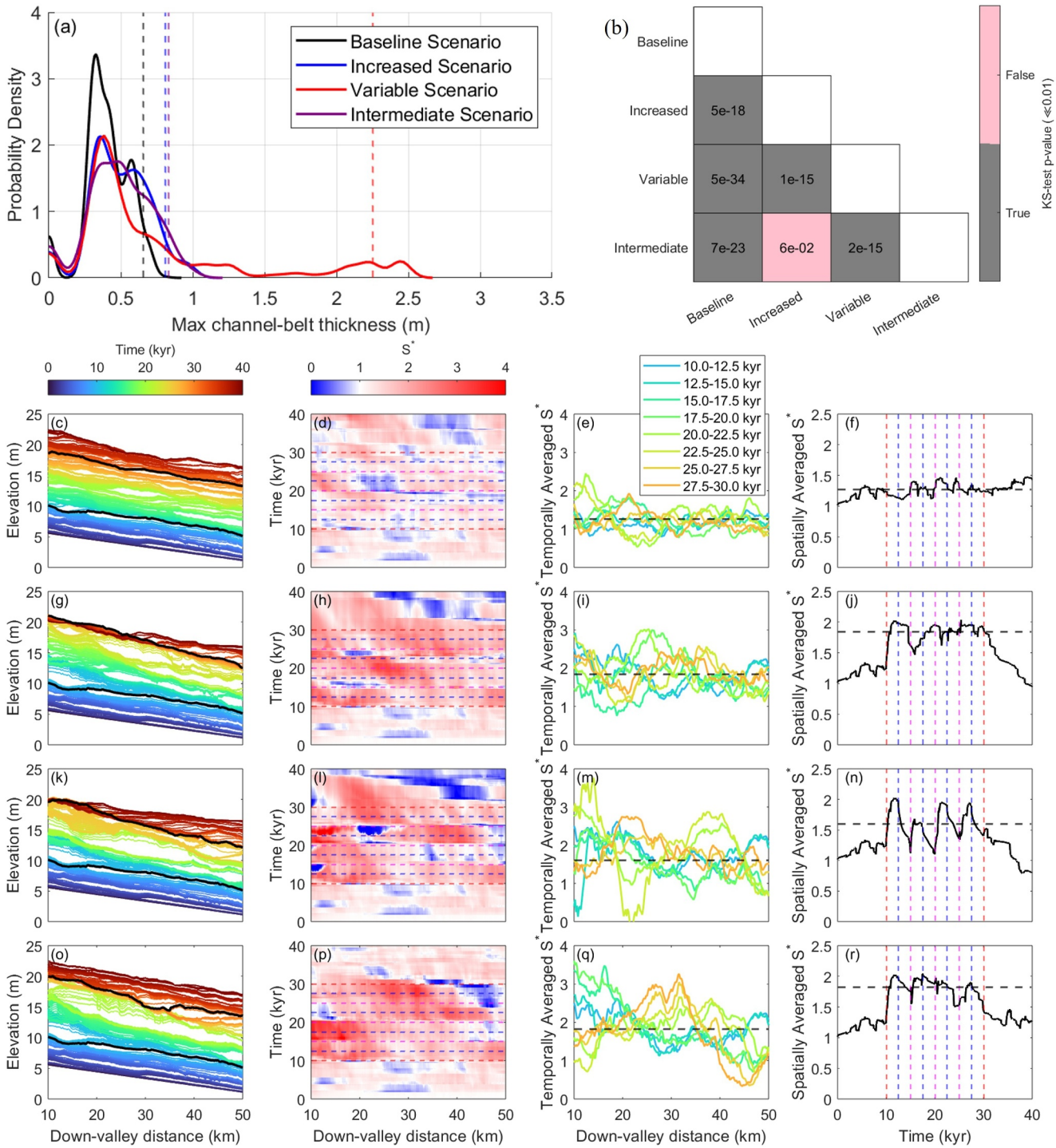

Figure 5. Comparison of maximum channel-belt thickness and dimensionless down-valley slope (S^*) across scenarios. (a) The kernel density estimates of maximum channel-belt thickness. Vertical dashed lines indicate the 95th percentile values for each scenario. (b) Pairwise Kolmogorov-Smirnov test results for maximum channel-belt thickness across the four scenarios, with $p \ll 0.01$ indicating statistically significant difference between two distributions. (c, g, k, o) Longitudinal surface topography along the basin axis ($y = 20$ km, Figure 1) shown at 50-year intervals. The two black solid lines represent $t = 10$ and 30 kyr, respectively, corresponding to the beginning and the end of the Q_s perturbation. (d, h, l, p) S^* variations over time and space. Horizontal lines are at a spacing of 2.5 kyr during the event. (e, i, m, q) Temporally-averaged dimensionless down-valley slope (S^*) values calculated for every 2.5 kyr interval, plotted against down-valley distances. The horizontal dashed line indicates the mean S^*, calculated as the average of the spatially averaged S^* values from all time intervals. (f, j, n, r) Spatially averaged S^* values computed across the entire length of down-valley distances (10–50 km) over the duration of the event. Vertical lines are at a spacing of 2.5 kyr during the event. The horizontal dashed line indicates the mean S^* during the event.

phase of the event as evidenced by the white dots during 25–30 kyr in Figure 3c. In contrast, variable sediment supply generates alternating intervals of aggradation and erosion corresponding directly to high and low sediment flux periods (Figure 3e–3h). This scenario is characterized by prolonged erosion and deposition phases and persistent channel belt activity in specific areas (Figures 3h and 3i). Notably, the overall stratigraphic pattern in this scenario is not dominantly aggradational; intense erosion can lower the topography at later times on a regional scale (see blue arrows in Figures 3h and 3i). The intermediate scenario exhibits alternating aggradation and degradation similar to the variable scenario, while its channel belt thickness remains visually comparable to that of the increased scenario (Figures 4b–4d).

3.2. Channel Belt Thickness

Channel belt thickness, estimated by the maximum incision depth from the PBTH algorithm (Section 2.3), shows pronounced differences across scenarios primarily at high percentiles. At the 95th percentile, thickness increases by 23% (to 0.81 m), 26% (0.83 m) and 241% (2.25 m) in the increased, intermediate and variable scenarios, respectively, relative to the baseline scenario (0.66 m) (Figure 5a). These increases diminish to 23%, 25%, and 58% at the 75th percentile, consistent with expectations of reduced differences among scenarios at less extreme thresholds. Median (50th percentile) thicknesses show minimal variation, ranging only between 0.40 and 0.49 m. These results indicate that high-magnitude, low-frequency events primarily drive stratigraphic contrasts, consistent with field observations of large PETM sandstone bodies mentioned in the Introduction. Identifying and measuring such extremes in the field, however, necessitates sufficiently extensive outcrop exposures. Two-sample Kolmogorov-Smirnov tests confirm statistically significant differences ($p \ll 0.01$) in thickness distributions for all scenario comparisons, except between the increased and intermediate scenarios (Figure 5b).

3.3. Down-Valley Slopes

Down-valley slopes differ notably between the sediment supply scenarios. In the baseline scenario, down-valley slopes remain stable over time, reflecting maintained equilibrium conditions, with temporally averaged dimensionless down-valley slopes (S^*) varying between 0.8 and 2.5 from upstream to downstream and spatial averages maintaining at around 1.25 (Figures 5c–5f). In contrast, the abrupt increase in sediment supply triggers an immediate, significant rise in down-valley slopes, particularly in the upstream region, maintaining persistently steeper down-valley slopes with mean spatially-averaged S^* of 1.80 throughout the event (Figures 5g–5j). The variable supply scenario shows the most dynamic response, with down-valley slopes fluctuating sharply between high and low sediment supply intervals, mirroring depositional and erosional phases. Temporally-averaged down-valley slopes locally peak at $S^* = 3.8$, while spatial averages alternate markedly around a mean S^* of 1.6, with an approximate oscillating periodicity of 5 kyr in line with the forcing (Figures 5k–5n). The intermediate scenario exhibits temporal and spatial variability that lies between the increased and variable scenarios (Figure 5q), with spatial averages fluctuating around a mean S^* of 1.8 and visually insignificant oscillating periodicity (Figure 5r). Two-sample Kolmogorov-Smirnov tests confirm statistically significant differences ($p \ll 0.01$) among distributions of all scenario pairs (Figure S2 in Supporting Information S1).

4. Discussion

4.1. Influence of Sediment Supply on Alluvial Architecture

Our modeling results demonstrate that the nature of sediment supply perturbations fundamentally influences alluvial stratigraphy. Specifically, when sediment supply varies temporally, the simulated fluvial system exhibits prolonged phases of alternating deposition and erosion (Figures 3f–3i). This regime significantly increases channel-belt thickness. By contrast, an abrupt, uniform increase in sediment supply leads to higher aggradation rates that trigger earlier channel avulsions, thereby constraining channel belt dimensions (Figures 3b–3d). These quantitative results refine our understanding of how distinct sediment supply regimes control channel-belt geometry and stratigraphic architecture, complementing and advancing previous studies (Bryant et al., 1995; Esposito et al., 2018; Fielding et al., 2018; Lyster et al., 2023; McLeod et al., 2023; Sharma et al., 2024; Straub & Wang, 2013; Wang et al., 2021).

Establishing these model-based relationships is crucial before tentatively comparing our findings to field observations. For instance, the significantly-enhanced channel sand-body thickness documented in the Bighorn

Basin (Foreman, 2014) may primarily reflect the impact of high sediment supply variability. In contrast, the minimal channel sand-body depth changes in the Tremp (Chen et al., 2018; Colombera et al., 2017), Piceance (Barefoot et al., 2022), and Hanna Basins (Dechesne et al., 2020) could result from increased sediment supply with limited variability.

For down-valley slopes, immediate accelerated aggradation is observed in upstream areas when sediment supply is initially increased. Consistently high sediment supply maintains steep down-valley slopes throughout the event, although intermittent decreases may occur due to the interplay between aggradation and accommodation creation (Figures 5c–5r). Conversely, variable supply produces alternating high and low down-valley slopes that directly mirror the phases of dominant deposition and erosion (Figures 3f–3i). The most pronounced down-valley slope adjustments occur in the upstream area at the onset of sediment supply perturbations, when the sudden sediment load temporarily exceeds the transport capacity of the system. Such spatially and temporally localized responses underscore the need to consider both basin locations and stratigraphic intervals when reconstructing down-valley slopes (Trampush & Hajek, 2017), which are often derived indirectly from grain size proxies and may vary over an order of magnitude (Barefoot et al., 2022).

4.2. Implications and Outlook

Our findings indicate that significantly thick channel belts may predominantly record variable sediment supply driven by climatic fluctuations rather than simply reflecting increases in total sediment supply. This distinction refines paleoenvironmental reconstructions of alluvial sediment records and enhances predictions of reservoir distribution within subsurface alluvial successions. For example, with increased total sediment supply, the development of smaller channels intercalated with overbank deposits suggests reduced reservoir connectivity and increased heterogeneity, conditions that can adversely affect fluid flow and resource extraction (Miall, 1988). In contrast, variable sediment supply produces thick channel sand-body with fewer fine-grained overbank deposits, thereby improving connectivity and homogenizing reservoir properties (Colombera et al., 2012; Gibling, 2006).

A deeper understanding of alluvial systems will require integration of additional dynamic processes into depositional models. Incorporating factors such as vegetation influences (Finotello et al., 2024; Ganti et al., 2019; Ielpi & Lapôtre, 2020; Vandenberghe, 2003), variable bank strengths (Parker et al., 2008; Simon & Collison, 2002), and floodplain-controlled avulsion thresholds (Edmonds et al., 2016; Gearon et al., 2024; Hajek & Wolinsky, 2012; Martin & Edmonds, 2022) will improve the realism of simulations. Coupling depositional models with erosional landscape evolution frameworks (e.g., Fastscape and Landlab; Braun & Willett, 2013; Hobley et al., 2017) and further with global climate models such as Community Earth System Model (CESM; Hurrell et al., 2013) offers a holistic approach that links atmospheric, hydrological, and sedimentary processes (Coulthard & Van de Wiel, 2013; Tucker & Hancock, 2010). Such integrations should be further combined with basin subsidence and sea-level change scenarios to simulate the response of specific alluvial systems to environmental perturbations.

5. Conclusions

Our stratigraphic forward modeling results show that temporal variability in sediment supply exerts a more pronounced influence on alluvial stratigraphic architecture than an abrupt increase in total sediment supply. Specifically, enhanced sediment supply variability produces thicker channel-belt deposits and alternating high and low down-valley slopes. In contrast, an abrupt increase in total sediment supply results in uniformly steep down-valley slopes with slightly changing channel belt thickness. Meanwhile, the down-valley slope alteration as a response to sediment supply change is highly dependent on the basin location and stratigraphic interval, with higher values in the upstream and near the onset of the supply increase. These findings underscore the differential impacts of sediment supply variability and magnitude on alluvial stratigraphy, which improves our ability to reconstruct past environments and predict future landscape evolution.

Data Availability Statement

MATLAB and Python codes and data used to generate the results of this study are available at Wang (2024).

Acknowledgments
This study was partially financially supported through the ROBUST project sponsored by Equinor to TU Delft, the Netherlands. We thank Allard Martinius, Joep Storms, and Cathrine Pedersen for discussion throughout that project; Ajay Limaye, Dimitri Bandou, and Vidushi Sharma for inspiring the application of the PBTH algorithm to channel mapping; David Kemp, Neil Ganju, James Gearon, and one anonymous reviewer for comments that helped to improve earlier versions of the manuscript.

References

Abels, H. A., Clyde, W. C., Gingerich, P. D., Hilgen, F. J., Fricke, H. C., Bowen, G. J., & Lourens, L. J. (2012). Terrestrial carbon isotope excursions and biotic change during Palaeogene hyperthermals. *Nature Geoscience*, *5*(5), 326–329. https://doi.org/10.1038/ngeo1427

Allen, P. A., Armitage, J. J., Carter, A., Duller, R. A., Michael, N. A., Sinclair, H. D., et al. (2013). The Qs problem: Sediment volumetric balance of proximal foreland basin systems. *Sedimentology*, *60*(1), 102–130. https://doi.org/10.1111/sed.12015

Armitage, J. J., Duller, R. A., Whittaker, A. C., & Allen, P. A. (2011). Transformation of tectonic and climatic signals from source to sedimentary archive. *Nature Geoscience*, *4*(4), 231–235. https://doi.org/10.1038/ngeo1087

Armitage, J. J., Dunkley Jones, T., Duller, R. A., Whittaker, A. C., & Allen, P. A. (2013). Temporal buffering of climate-driven sediment flux cycles by transient catchment response. *Earth and Planetary Science Letters*, *369–370*, 200–210. https://doi.org/10.1016/j.epsl.2013.03.020

Barefoot, E. A., Nittrouer, J. A., Foreman, B. Z., Hajek, E. A., Dickens, G. R., Baisden, T., & Toms, L. (2022). Evidence for enhanced fluvial channel mobility and fine sediment export due to precipitation seasonality during the Paleocene-Eocene thermal maximum. *Geology*, *50*(1), 116–120. https://doi.org/10.1130/G49149.1

Blum, M. D., & Hattier-Womack, J. (2009). *Climate change, sea-level change, and fluvial sediment supply to deepwater depositional systems, external controls on deep-water depositional systems* (Vol. 92, pp. 15–39). SEPM Special Publication. https://doi.org/10.2110/sepmsp.092.015

Blum, M. D., & Törnqvist, T. E. (2000). Fluvial responses to climate and sea-level change: A review and look forward. *Sedimentology*, *47*(s1), 2–48. https://doi.org/10.1046/j.1365-3091.2000.00008.x

Braun, J., & Willett, S. D. (2013). A very efficient O(n), implicit and parallel method to solve the stream power equation governing fluvial incision and landscape evolution. *Geomorphology*, *180–181*, 170–179. https://doi.org/10.1016/j.geomorph.2012.10.008

Bridge, J. S., & Leeder, M. R. (1979). A simulation model of alluvial stratigraphy. *Sedimentology*, *26*(5), 617–644. https://doi.org/10.1111/j.1365-3091.1979.tb00935.x

Bryant, M., Falk, P., & Paola, C. (1995). Experimental study of avulsion frequency and rate of deposition. *Geology*, *23*(4), 365. https://doi.org/10.1130/0091-7613(1995)023<0365:ESOAFA>2.3.CO;2

Burgess, P., Masiero, I., Toby, S., & Duller, R. (2019). A big fan of signals? Exploring autogenic and Allogenic process and product in a numerical stratigraphic forward model of submarine-fan development. *Journal of Sedimentary Research*, *89*, 1–12. https://doi.org/10.2110/jsr.2019.3

Carmichael, M. J., Inglis, G. N., Badger, M. P. S., Naafs, B. D. A., Behrooz, L., Remmelzwaal, S., et al. (2017). Hydrological and associated biogeochemical consequences of rapid global warming during the Paleocene-Eocene thermal maximum. *Global and Planetary Change*, *157*, 114–138. https://doi.org/10.1016/j.gloplacha.2017.07.014

Castelltort, S., & Van Den Driessche, J. (2003). How plausible are high-frequency sediment supply-driven cycles in the stratigraphic record? *Sedimentary Geology*, *157*(1–2), 3–13. https://doi.org/10.1016/S0037-0738(03)00066-6

Catuneanu, O., Galloway, W., Kendall, C., Miall, A., Posamentier, H., Strasser, A., & Tucker, M. (2011). Sequence stratigraphy: Methodology and nomenclature. *Newsletters on Stratigraphy*, *44*(3), 173–245. https://doi.org/10.1127/0078-0421/2011/0011

Chen, C., Guerit, L., Foreman, B. Z., Hassenruck-Gudipati, H. J., Adatte, T., Honegger, L., et al. (2018). Estimating regional flood discharge during Palaeocene-Eocene global warming. *Scientific Reports*, *8*(1), 13391. https://doi.org/10.1038/s41598-018-31076-3

Colombera, L., Arévalo, O. J., & Mountney, N. P. (2017). Fluvial-system response to climate change: The Paleocene-Eocene tremp group, Pyrenees, Spain. *Global and Planetary Change*, *157*, 1–17. https://doi.org/10.1016/j.gloplacha.2017.08.011

Colombera, L., Mountney, N. P., & McCaffrey, W. D. (2012). A relational database for the digitization of fluvial architecture: Concepts and example applications. *Petroleum Geoscience*, *18*(1), 129–140. https://doi.org/10.1144/1354-079311-021

Conover, W. J. (1999). *Practical nonparametric statistics* (3rd ed.). John Wiley and Sons.

Coulthard, T. J., & Van de Wiel, M. J. (2013). Climate, tectonics or morphology: What signals can we see in drainage basin sediment yields? *Earth Surface Dynamics*, *1*(1), 13–27. https://doi.org/10.5194/esurf-1-13-2013

Dechesne, M., Currano, E. D., Dunn, R. E., Higgins, P., Hartman, J. H., Chamberlain, K. R., & Holm-Denoma, C. S. (2020). A new stratigraphic framework and constraints for the position of the Paleocene–Eocene boundary in the rapidly subsiding Hanna Basin, Wyoming. *Geosphere*, *16*(2), 594–618. https://doi.org/10.1130/GES02118.1

Duller, R. A., Armitage, J. J., Manners, H. R., Grimes, S., & Jones, T. D. (2019). Delayed sedimentary response to abrupt climate change at the Paleocene-Eocene boundary, northern Spain. *Geology*, *47*(2), 159–162. https://doi.org/10.1130/G45631.1

Edmonds, D. A., Hajek, E. A., Downton, N., & Bryk, A. B. (2016). Avulsion flow-path selection on rivers in foreland basins. *Geology*, *44*(9), 695–698. https://doi.org/10.1130/G38082.1

Esposito, C. R., Di Leonardo, D., Harlan, M., & Straub, K. M. (2018). Sediment storage partitioning in alluvial stratigraphy: The influence of discharge variability. *Journal of Sedimentary Research*, *88*(6), 717–726. https://doi.org/10.2110/jsr.2018.36

Fielding, C. R., Alexander, J., & Allen, J. P. (2018). The role of discharge variability in the formation and preservation of alluvial sediment bodies. *Sedimentary Geology*, *365*, 1–20. https://doi.org/10.1016/j.sedgeo.2017.12.022

Finotello, A., Ielpi, A., Lapôtre, M. G. A., Lazarus, E. D., Ghinassi, M., Carniello, L., et al. (2024). Vegetation enhances curvature-driven dynamics in meandering rivers. *Nature Communications*, *15*(1), 1968. https://doi.org/10.1038/s41467-024-46292-x

Foreman, B. Z. (2014). Climate-driven generation of a fluvial sheet sand body at the Paleocene-Eocene boundary in north-west Wyoming (USA). *Basin Research*, *26*(2), 225–241. https://doi.org/10.1111/bre.12027

Foreman, B. Z., Heller, P. L., & Clementz, M. T. (2012). Fluvial response to abrupt global warming at the Palaeocene/Eocene boundary. *Nature*, *491*(7422), 92–95. https://doi.org/10.1038/nature11513

Foreman, B. Z., & Straub, K. M. (2017). Autogenic geomorphic processes determine the resolution and fidelity of terrestrial paleoclimate records. *Science Advances*, *3*(9), e1700683. https://doi.org/10.1126/sciadv.1700683

Ganti, V., Whittaker, A. C., Lamb, M. P., & Fischer, W. W. (2019). Low-gradient, single-threaded rivers prior to greening of the continents. *Proceedings of the National Academy of Sciences*, *116*(24), 11652–11657. https://doi.org/10.1073/pnas.1901642116

Gearon, J. H., Martin, H. K., DeLisle, C., Barefoot, E. A., Mohrig, D., Paola, C., & Edmonds, D. A. (2024). Rules of river avulsion change downstream. *Nature*, *634*(8032), 91–95. https://doi.org/10.1038/s41586-024-07964-2

Gibling, M. (2006). Width and thickness of fluvial channel bodies and valley fills in the geological record: A literature compilation and classification. *Journal of Sedimentary Research*, *76*(5), 731–770. https://doi.org/10.2110/jsr.2006.060

Hajek, E. A., & Straub, K. M. (2017). Autogenic sedimentation in clastic stratigraphy. *Annual Review of Earth and Planetary Sciences*, *45*(1), 681–709. https://doi.org/10.1146/annurev-earth-063016-015935

Hajek, E. A., & Wolinsky, M. A. (2012). Simplified process modeling of river avulsion and alluvial architecture: Connecting models and field data. *Sedimentary Geology*, *257–260*, 1–30. https://doi.org/10.1016/j.sedgeo.2011.09.005

Hobley, D. E. J., Adams, J. M., Nudurupati, S. S., Hutton, E. W. H., Gasparini, N. M., Istanbulluoglu, E., & Tucker, G. E. (2017). Creative computing with landlab: An open-source toolkit for building, coupling, and exploring two-dimensional numerical models of Earth-surface dynamics. *Earth Surface Dynamics*, *5*(1), 21–46. https://doi.org/10.5194/esurf-5-21-2017

Hurrell, J. W., Holland, M. M., Gent, P. R., Ghan, S., Kay, J. E., Kushner, P. J., et al. (2013). The community Earth system model: A framework for collaborative research. *Bulletin of the American Meteorological Society*, *94*(9), 1339–1360. https://doi.org/10.1175/BAMS-D-12-00121.1

Ielpi, A., & Lapôtre, M. G. A. (2020). A tenfold slowdown in river meander migration driven by plant life. *Nature Geoscience*, *13*(1), 82–86. https://doi.org/10.1038/s41561-019-0491-7

Jerolmack, D. J., & Paola, C. (2010). Shredding of environmental signals by sediment transport. *Geophysical Research Letters*, *37*(19). https://doi.org/10.1029/2010GL044638

Jin, S., Kemp, D. B., Jolley, D. W., Vieira, M., Zachos, J. C., Huang, C., et al. (2022). Large-scale, astronomically paced sediment input to the North Sea Basin during the Paleocene Eocene thermal maximum. *Earth and Planetary Science Letters*, *579*, 117340. https://doi.org/10.1016/j.epsl.2021.117340

Karssenberg, D., & Bridge, J. S. (2008). A three-dimensional numerical model of sediment transport, erosion and deposition within a network of channel belts, floodplain and hill slope: Extrinsic and intrinsic controls on floodplain dynamics and alluvial architecture. *Sedimentology*, *55*(6), 1717–1745. https://doi.org/10.1111/j.1365-3091.2008.00965.x

Limaye, A. B. (2020). How do braided rivers grow channel belts? *Journal of Geophysical Research: Earth Surface*, *125*(8), e2020JF005570. https://doi.org/10.1029/2020JF005570

Luo, W., Pingel, T., Heo, J., Howard, A., & Jung, J. (2015). A progressive black top hat transformation algorithm for estimating valley volumes on Mars. *Computers and Geosciences*, *75*, 17–23. https://doi.org/10.1016/j.cageo.2014.11.003

Lyster, S. J., Whittaker, A. C., Farnsworth, A., & Hampson, G. J. (2023). Constraining flow and sediment transport intermittency in the geological past. *Geological Society of America Bulletin*. https://doi.org/10.1130/B36873.1

Mackey, S. D., & Bridge, J. S. (1995). Three-dimensional model of alluvial stratigraphy; theory and applications. *Journal of Sedimentary Research*, *65*(1b), 7–31. https://doi.org/10.1306/D42681D5-2B26-11D7-8648000102C1865D

Martin, H., & Edmonds, D. (2022). The push and pull of abandoned channels: How floodplain processes and healing affect avulsion dynamics and alluvial landscape evolution in foreland basins. *Earth Surface Dynamics*, *10*(3), 555–579. https://doi.org/10.5194/esurf-10-555-2022

McLeod, J. S., Wood, J., Lyster, S. J., Valenza, J. M., Spencer, A. R. T., & Whittaker, A. C. (2023). Quantitative constraints on flood variability in the rock record. *Nature Communications*, *14*(1), 3362. https://doi.org/10.1038/s41467-023-38967-8

Miall, A. D. (1988). Reservoir heterogeneities in fluvial sandstones: Lessons from outcrop studies. *AAPG Bulletin*, *72*(6), 682–697. https://doi.org/10.1306/703C8F01-1707-11D7-8645000102C1865D

Muto, T., & Steel, R. (1997). Principles of regression and transgression: The nature of the interplay between accommodation and sediment supply. *Journal of Sedimentary Research*, *67*(6), 994–1000. https://doi.org/10.1306/D42686A8-2B26-11D7-8648000102C1865D

Neal, J., & Abreu, V. (2009). Sequence stratigraphy hierarchy and the accommodation succession method. *Geology*, *37*(9), 779–782. https://doi.org/10.1130/G25722A.1

Parker, C., Simon, A., & Thorne, C. R. (2008). The effects of variability in bank material properties on riverbank stability: Goodwin Creek, Mississippi. *Geomorphology*, *101*(4), 533–543. https://doi.org/10.1016/j.geomorph.2008.02.007

Podrecca, L. G., Makarova, M., Miller, K. G., Browning, J. V., & Wright, J. D. (2021). Clear as mud: Clinoform progradation and expanded records of the Paleocene-Eocene Thermal Maximum. *Geology*, *49*(12), 1441–1445. https://doi.org/10.1130/G49061.1

Prieur, M., Robin, C., Braun, J., Vaucher, R., Whittaker, A., Jaimes Gutiérrez, R., et al. (2025). Climate control on erosion: Evolution of sediment flux from mountainous catchments during a global warming event, PETM, Southern Pyrenees, Spain. *Geophysical Research Letters*, *52*(7), e2024GL112404. https://doi.org/10.1029/2024GL112404

Prieur, M., Whittaker, A. C., Nuriel, P., Jaimes-Gutierrez, R., Garzanti, E., Roigé, M., et al. (2024). Fingerprinting enhanced floodplain reworking during the paleocene−eocene Thermal Maximum in the Southern Pyrenees (Spain): Implications for channel dynamics and carbon burial. *Geology*, *52*(9), 651–655. https://doi.org/10.1130/G52180.1

Pujalte, V., Baceta, J. I., & Schmitz, B. (2015). A massive input of coarse-grained siliciclastics in the Pyrenean Basin during the PETM: The missing ingredient in a coeval abrupt change in hydrological regime. *Climate of the Past*, *11*(12), 1653–1672. https://doi.org/10.5194/cp-11-1653-2015

Romans, B. W., Castelltort, S., Covault, J. A., Fildani, A., & Walsh, J. P. (2016). Environmental signal propagation in sedimentary systems across timescales. *Earth-Science Reviews*, *153*, 7–29. https://doi.org/10.1016/j.earscirev.2015.07.012

Schmitz, B., & Pujalte, V. (2007). Abrupt increase in seasonal extreme precipitation at the Paleocene-Eocene boundary. *Geology*, *35*(3), 215. https://doi.org/10.1130/G23261A.1

Shanley, K. W., & McCabe, P. (1994). Perspectives on the sequence stratigraphy of Continental strata. *AAPG Bulletin*, *78*. https://doi.org/10.1306/BDFF9258-1718-11D7-8645000102C1865D

Sharma, N., Adatte, T., & Castelltort, S. (2024). Water discharge and sediment flux intermittency in the fluvial Escanilla formation, Spain: Implications for changes in stratigraphic architecture. *The Depositional Record*, *10*(1), 245–259. https://doi.org/10.1002/dep2.272

Sharman, G., Szymanski, E., Hackworth, R., Kahn, A., Febo, L., Oefinger, J., & Gregory, G. (2022). Carbon-isotope chemostratigraphy, geochemistry, and biostratigraphy of the Paleocene-Eocene thermal maximum, deep-water wilcox group, Gulf of Mexico (U.S.A.). https://doi.org/10.5194/cp-2022-86

Simon, A., & Collison, A. J. C. (2002). Quantifying the mechanical and hydrologic effects of riparian vegetation on streambank stability. *Earth Surface Processes and Landforms*, *27*(5), 527–546. https://doi.org/10.1002/esp.325

Simpson, G., & Castelltort, S. (2012). Model shows that Rivers transmit high-frequency climate cycles to the sedimentary record. *Geology*, *40*(12), 1131–1134. https://doi.org/10.1130/G33451.1

Sømme, T. O., Huwe, S. I., Martinsen, O. J., Sandbakken, P. T., Skogseid, J., & Valore, L. A. (2023). Stratigraphic expression of the Paleocene-Eocene thermal maximum climate event during long-lived transient uplift—An example from a shallow to deep-marine clastic system in the Norwegian Sea. *Frontiers in Earth Science*, *11*, 1082203. https://doi.org/10.3389/feart.2023.1082203

Straub, K. M., Duller, R. A., Foreman, B. Z., & Hajek, E. A. (2020). Buffered, incomplete, and shredded: The challenges of reading an imperfect stratigraphic record. *Journal of Geophysical Research: Earth Surface*, *125*(3), e2019JF005079. https://doi.org/10.1029/2019JF005079

Straub, K. M., & Wang, Y. (2013). Influence of water and sediment supply on the long-term evolution of alluvial fans and deltas: Statistical characterization of basin-filling sedimentation patterns. *Journal of Geophysical Research: Earth Surface*, *118*(3), 1602–1616. https://doi.org/10.1002/jgrf.20095

Syvitski, J. P., Morehead, M. D., Bahr, D. B., & Mulder, T. (2000). Estimating fluvial sediment transport: The rating parameters. *Water Resources Research*, *36*(9), 2747–2760. https://doi.org/10.1029/2000WR900133

Tierney, J. E., Zhu, J., Li, M., Ridgwell, A., Hakim, G. J., Poulsen, C. J., et al. (2022). Spatial patterns of climate change across the Paleocene–Eocene thermal maximum. *Proceedings of the National Academy of Sciences*, *119*(42), e2205326119. https://doi.org/10.1073/pnas.2205326119

Toby, S. C., Duller, R. A., De Angelis, S., & Straub, K. M. (2019). A stratigraphic framework for the preservation and shredding of environmental signals. *Geophysical Research Letters*, *46*(11), 5837–5845. https://doi.org/10.1029/2019GL082555

Trampush, S. M., & Hajek, E. A. (2017). Preserving proxy records in dynamic landscapes: Modeling and examples from the Paleocene-Eocene Thermal Maximum. *Geology*, *45*(11), 967–970. https://doi.org/10.1130/g39367.1

Tucker, G. E., & Hancock, G. R. (2010). Modelling landscape evolution. *Earth Surface Processes and Landforms*, *35*(1), 28–50. https://doi.org/10.1002/esp.1952

Vandenberghe, J. (2003). Climate forcing of fluvial system development: An evolution of ideas. *Quaternary Science Reviews*, *22*(20), 2053–2060. https://doi.org/10.1016/S0277-3791(03)00213-0

van der Meulen, B., Gingerich, P. D., Lourens, L. J., Meijer, N., van Broekhuizen, S., van Ginneken, S., & Abels, H. A. (2020). Carbon isotope and mammal recovery from extreme greenhouse warming at the Paleocene–Eocene boundary in astronomically-calibrated fluvial strata, Bighorn Basin, Wyoming, USA. *Earth and Planetary Science Letters*, *534*, 116044. https://doi.org/10.1016/j.epsl.2019.116044

Vimpere, L., Spangenberg, J., Roige, M., Adatte, T., De Kaenel, E., Fildani, A., et al. (2023). Carbon isotope and biostratigraphic evidence for an expanded Paleocene–Eocene Thermal Maximum sedimentary record in the deep Gulf of Mexico. *Geology*, *51*(4), 334–339. https://doi.org/10.1130/G50641.1

Wang, Y. (2024). Data and code for modeling alluvial stratigraphic response to abruptly increasing and variable sediment supply [Dataset]. *Zenodo*. https://doi.org/10.5281/zenodo.13211457

Wang, Y., Baars, T. F., Storms, J. E. A., Martinius, A. W., Gingerich, D., Chmielewska, M., et al. (2023). Lateral and vertical characteristics of floodplain aggradation cycles in the lower Eocene willwood formation, bighorn basin, Wyoming, USA. *Geological Society of America Bulletin*, *136*(5–6), 2568–2581. https://doi.org/10.1130/B36908.1

Wang, Y., Baars, T. F., Storms, J. E. A., Martinius, A. W., Gingerich, P. D., & Abels, H. A. (2024). Long-eccentricity pacing of alluvial stratigraphic architecture in the Eocene bighorn basin, Wyoming, USA. *Geology*, *52*(8), 588–593. https://doi.org/10.1130/G52131.1

Wang, Y., Storms, J. E. A., Martinius, A. W., Karssenberg, D., & Abels, H. A. (2021). Evaluating alluvial stratigraphic response to cyclic and non-cyclic upstream forcing through process-based alluvial architecture modelling. *Basin Research*, *33*(1), 48–65. https://doi.org/10.1111/bre.12454

Zachos, J. C., McCarren, H., Murphy, B., Röhl, U., & Westerhold, T. (2010). Tempo and scale of late Paleocene and early Eocene carbon isotope cycles: Implications for the origin of hyperthermals. *Earth and Planetary Science Letters*, *299*(1–2), 242–249. https://doi.org/10.1016/j.epsl.2010.09.004

Zhang, J., Burgess, P. M., Granjeon, D., & Steel, R. (2019). Can sediment supply variations create sequences? Insights from stratigraphic forward modelling. *Basin Research*, *31*(2), 274–289. https://doi.org/10.1111/bre.12320